Supplementary material

Super adsorption capability and excellent photocatalytic activity derived from the ferroelectric external screening effect in Bi$_3$TiNbO$_9$ single-crystal nanosheets

Xiaofeng Yin,*[a,b] Yingjie Sun,[d] Xiaojun Wu,[b,c] Xiaoning Li,[b] Huan Liu,[b] Wen Gu,[b] Wei Zou,[b] Liuyang Zhu,[b] Zhengping Fu,*[b,c] and Yalin Lu*[b,c]

[a.]Henan Collaborative Innovation Center of Energy-Saving Building Materials, Xinyang Normal University, Xinyang 464000, China

[b.]Department of Materials Science and Engineering, CAS Key Laboratory of Materials for Energy Conversion, University of Science and Technology of China, Hefei 230026, P. R. China

[c.]Synergetic Innovation Center of Quantum Information and Quantum Physics & Hefei National Laboratory for Physical Sciences at Microscale, University of Science and Technology of China, Hefei 230026, P. R. China

[d.]School of Science, Hebei University of Science and Technology, Shijiazhuang, Hebei 050018, China

Corresponding Authors

*E-mail: yxfeng@xynu.edu.cn; fuzp@ustc.edu.cn; yllu@ustc.edu.cn

Computational method

Our simulations were performed by using density functional theory (DFT) implemented in Vienna ab initio Simulation Package (VASP)[1,2]. The interactions between cores and valence electrons were described by the projector augmented wave (PAW) method[3]. The exchange and correlation terms were treated with the generalized gradient approximation Perdew−Burke−Ernzerhof revised for solids (PBEsol)[4]. The kinetic energy cutoff was set as 500eV and the first Brillouin Zone is sampled with a k-point mesh of 9×9×2 by using Monkhorst–Packing scheme. For geometry optimization, both the lattice contents and the atomic positions were fully relaxed until the force is less than $10^{-2}e$V/Å. The convergence criterion of energy was set to be smaller than 10^{-5} eV. The Berry phase method was employed for the crystalline polarization[5,6].

Results and discussion

Our systematic calculation begins with the geometric details of Bi_3TiNbO_9 (BTNO) structure with *A21am* orthorhombic symmetry provided by experimental parameters, in which the Ti and Nb atoms occupying the same positons of perovskite B sites with a stoichiometric ratio 1:1. Notably, VASP can not directly calculate those systems that the atomic positions are not 100% occupied by the same elements. Considering this case, we design eight possible configurations depicted in Figure S1 by distributing four Nb and four Ti atoms over these eight B sites. The configurations are grouped into inner and outer mixed. The first category including a to e listed in Figure S1 shows that each perovskite layer contains both Ti and Nb atoms, the second one containing f to g refers to that the B sites of each layer are the same elements. In order to identify a possible site preference of the Ti^{4+} and Nb^{5+} cations, the relative energies for all the structures are compared Table S1, It is clear that the configurations of d has the lowest energy, in which the octahedral TiO_6 and NbO_6 stack in order of TNNTNTTN along c axis from the view of 100 directions, where the T and N represent the TiO_6 and NbO_6 octahedrons, respectively. The optimized lattice constants for the structure of d are a=5.37Å, b=5.35 Å and c=25.66 Å, consistent with the experimental values. We then estimate the spontaneous polarization based on

Berry phase calculation method, The results show that the spontaneous polarization in ab-plane is about 4.28 $\mu C \cdot cm^{-2}$, and the spontaneous polarization along c axis is only about $1.3 \times 10^{-4} \mu C \cdot cm^{-2}$, which is also in good agreement with the experimental phenomena. The spontaneous polarization of other configurations with higher energies were also calculated, it obviously shows that the spontaneous polarization in ab-plane contributes the most, and the polarization along c directions is much less except the configurations of c and g ,which is about 1.41 and 1.95 $\mu C \cdot cm^{-2}$,rexpectively.
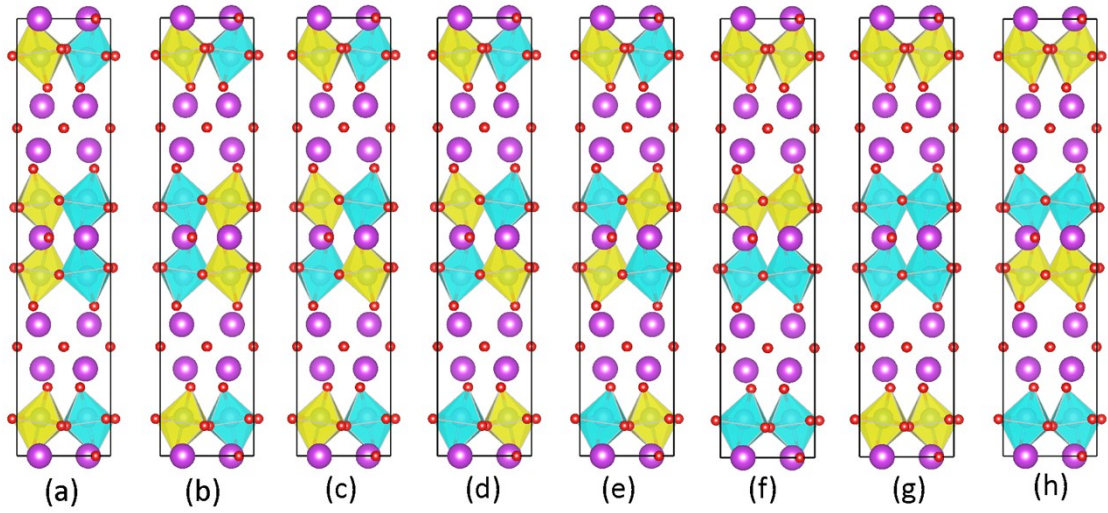

Figure S1. The eight configurations considered in this work from the perspective view of 100 directions, corresponding to different distributions of Nb and Ti over the octahedral B sites. Nb and Ti sites are indicated by yellow and cyan octahedra, respectively.

| configuration	1	2	3	4	5	6	7	8
$\Delta E(eV)$	0.417	0.568	0.458	0	0.310	0.550	2.011	1.598
$P_a(\mu C/cm^2)$	2.3	2.15	1.12	4.28	3.02	0.17	/	3.49
$P_b(\mu C/cm^2)$	0	3.6	3.30	2.18E-05	2.15E-05	2.13E-05	/	4.26E-05
$P_c(\mu C/cm^2)$	0	0	1.41	1.31E-04	1.72E-03	8.50E-05	/	1.95

Table S1. The relative energies (ΔE, in unit of eV) and pontaneous polarization (P,in unit of μC/cm²) for the eight configurations are summarized.
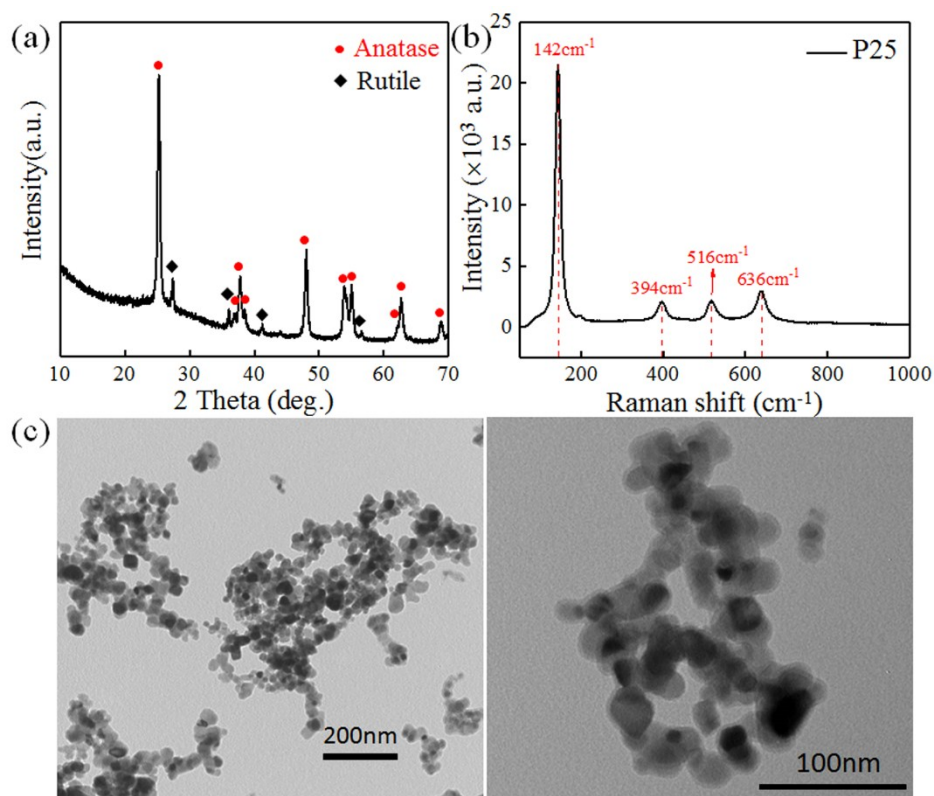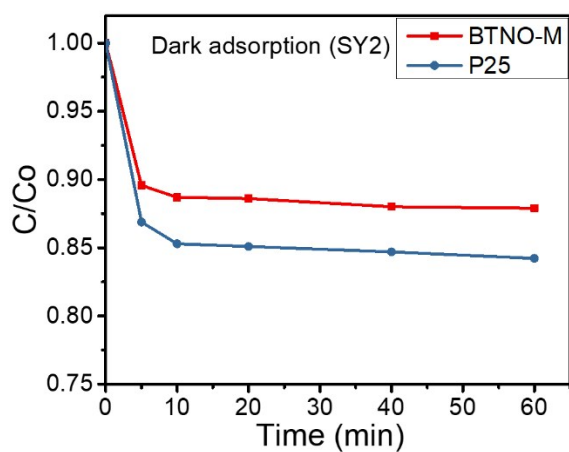
Figure S2. (a) The XRD diffraction spectra of the purchased P25; (b) Raman scattering spectra of the purchased P25; (c) TEM images of the purchased P25.
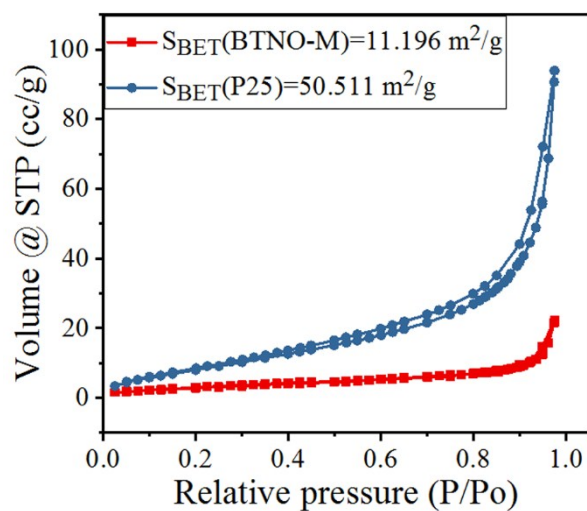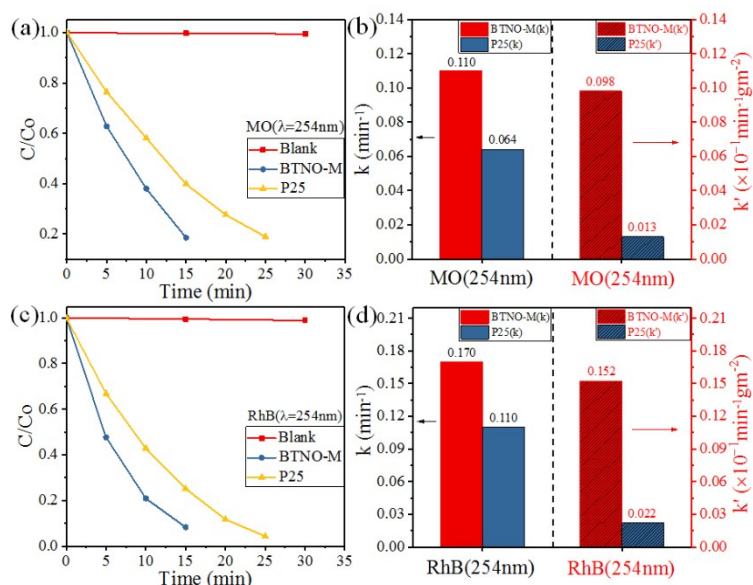

**Figure S3.** Nitrogen adsorption-desorption isotherm of BTNO-M and P25.
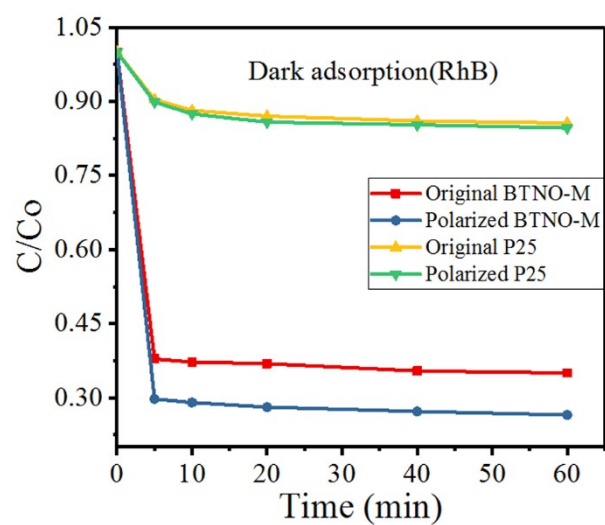
Figure S4. The dark absorption curves of original BTNO-M, polarized BTNO-M, original P25 and polarized P25.


**Figure S5** The SY2 dark absorption curves of BTNO-M and P25.

Figure S6. (a) The MO degradation curves of blank, BTNO-M and P25 under UV-light irradiation (λ=254 nm) without dark reaction; (b) The corresponding MO degradation kinetic constants k and normalized kinetic constants k′ of BTNO-M and P25 under UV-light irradiation (λ=254 nm); (c) The RhB degradation curves of blank, BTNO-M and P25 under UV-light irradiation (λ=254 nm) without dark reaction; (d) The corresponding RhB degradation kinetic constants k and normalized kinetic constants k′ of BTNO-M and P25 under UV-light irradiation (λ=254 nm).
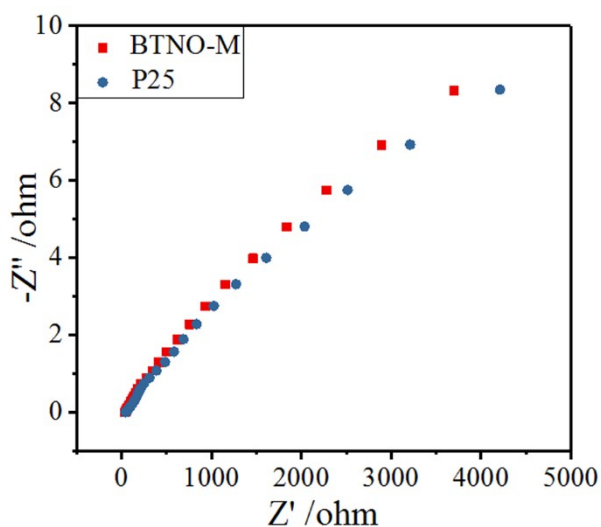

**Figure S7.** The electrochemical impedance spectroscopy of BTNO-M and P25.
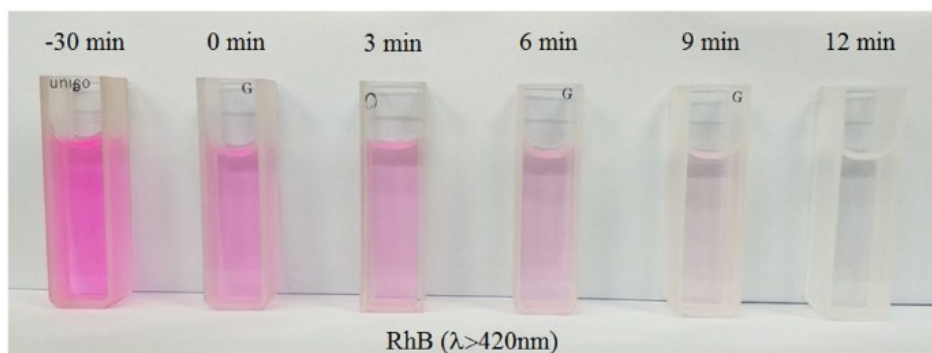
Figure S8. The photographs of the supernatant after RhB photosensitization degradation (BTNO-M samples λ>420 nm).
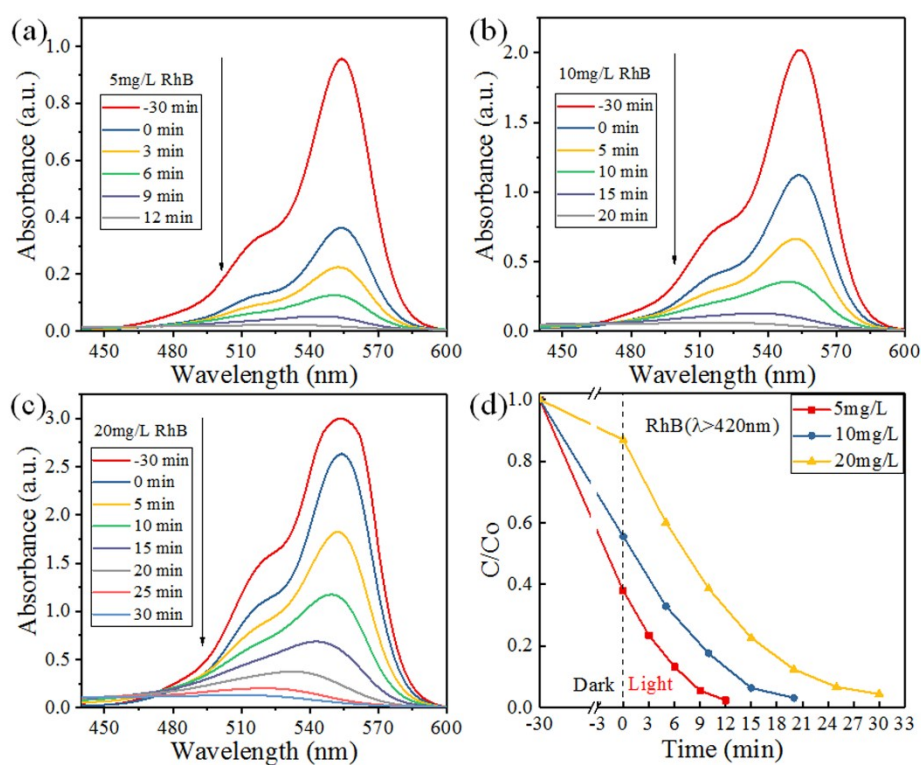

Figure S9. (a, b, c) UV-vis spectral changes with time of RhB (5 mg/L, 10 mg/L, 20 mg/L) sampled from RhB/BTNO-M suspension under visible-light irradiation (λ>420 nm); (d) Photosensitization degradation curves (BTNO-M samples) of RhB (5 mg/L, 10 mg/L, 20 mg/L) under visible-light irradiation (λ>420 nm).
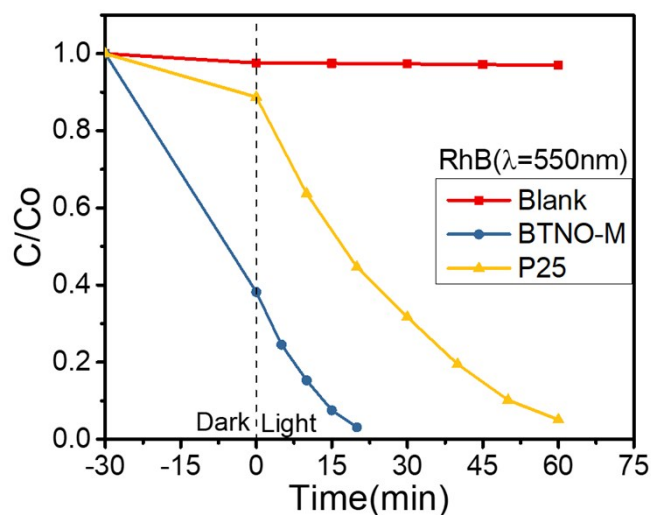
Figure S10 The RhB degradation curves of blank (without a catalyst), BTNO-M and P25 under visible-light irradiation (λ=550 nm).
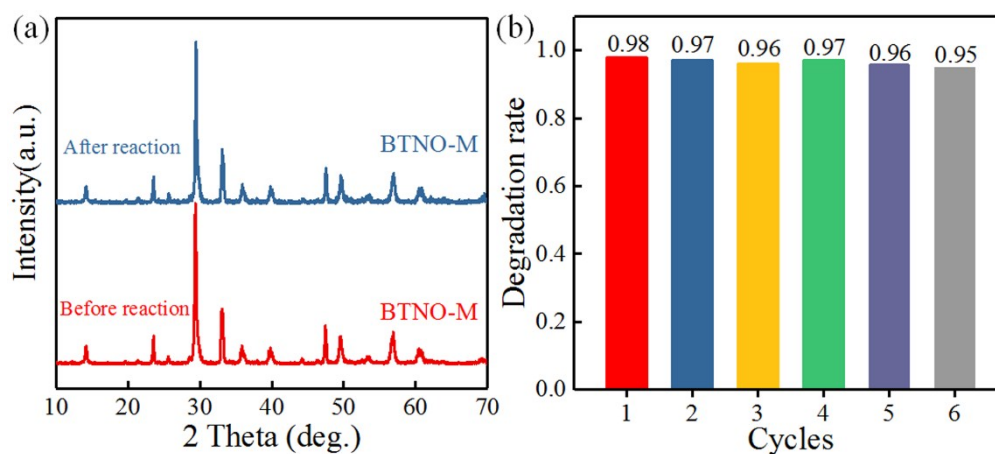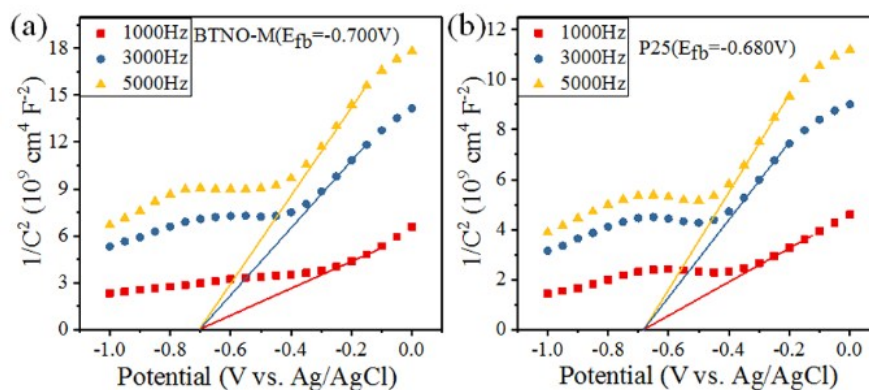

Figure S11. (a) The XRD diffraction spectra of BTNO-M samples before and after the photocatalytic reaction; (b) Cyclic photodegradation comparison experiments of BTNO-M samples.
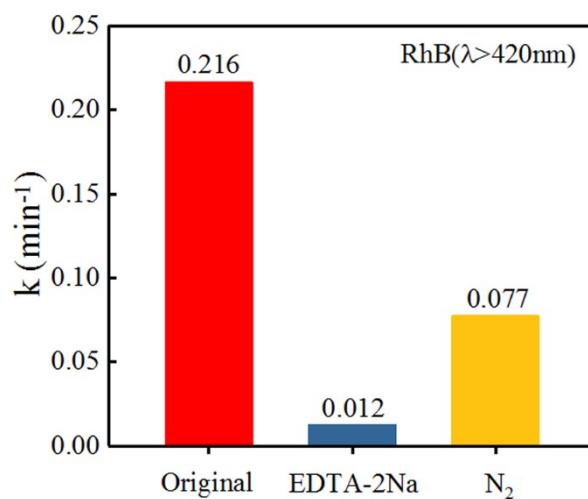
Figure S12. The RhB photosensitization degradation (λ>420 nm) kinetic constants k of original BTNO-M, the addition of EDTA-2Na and the introduction of N_2.

Figure S13. The Mott-Schottky curves of BTNO-M and P25.

References

1. G. Kresse, J. Furthmüller, *Comput. Mater. Sci.*, 1996, **6**, 15-50.
2. P. Käckell, J. Furthmüller, F. Bechstedt, G. Kresse, J. Hafner, *Phys. Rev. B*, 1996, **54**, 10304.
3. J. J. Mortensen, L. B. Hansen, K. W. Jacobsen, *Phys. Rev. B*, 2005, **71**, 035109.
4. J. P. Perdew, A. Ruzsinszky, G. I. Csonka, O. A. Vydrov, G. E. Scuseria, L. A. Constantin, X. Zhou, K. Burke, *Phys. Rev. Lett.*, 2008, **100**, 136406.
5. R. D. King-Smith, D. Vanderbilt, *Phys. Rev. B*, 1993, **47**, 1651.
6. R. Resta, M. Posternak, A. Baldereschi, *Phys. Rev. Lett.*, 1993, **70**, 1010.